JMEPEG (2009) 18:631–637
DOI: 10.1007/s11665-009-9395-9

1059-9495/$19.00

Numerical Study on the Influence of Material Characteristics on Ni-Ti Endodontic Instrument Performance

Lorenza Petrini, Silvia Necchi, Silvio Taschieri, and Francesco Migliavacca

(Submitted September 24, 2008; in revised form January 20, 2009)

Ni-Ti rotary endodontic instruments (*files*) are used in dentistry during the endodontic treatment to shape the root canal of the tooth while removing the pulp when infected. Up to now, the studies for evaluating their performances and drawbacks were mainly limited to experimental tests on product flexural and torsional resistance. This work exploits computational analyses for investigating the effects of materials with different mechanical properties on the behavior of rotary endodontic instruments. The aim is to understand the appropriate material choice to reduce the criticality of the treatment in particular clinical conditions. In particular, the interaction between an accurately modeled rotating file and differently shaped root canals during the clinical procedure was studied performing finite element analyses. Strains induced by the treatment on a file made of a "standard" Ni-Ti alloy (characterized by average properties of the pseudoelastic behavior), a "long" Ni-Ti alloy (characterized by wide transformation region), a "super" Ni-Ti alloy (characterized by an extended Hookian behavior without transformation region), and stainless steel were compared. The results accurately show the advantages of the use of Ni-Ti alloy with respect to stainless steel and the better performance of the "long" alloy in all the tested case.

Keywords endodontic files, finite element method, ProTaper, pseudoelasticity, shape memory alloys

1. Introduction

Endodontics is the field of dentistry dealing with problems of the pulp, the living tissue contained in the root canal of the tooth (Fig. 1a). Rotary endodontic instruments (also called *endodontic files*) are used during the endodontic treatment (Fig. 1b-d) to shape the root canal while removing the pulp when infected. A good shaping of the canal is mandatory to allow its efficient cleaning and obturation and to ensure the success of the treatment. Endodontic instruments must show a good flexibility and a cutting profile to be able to penetrate in the root canal and to remove dentin; therefore, they result in a sort of thin and flexible drill bit (Fig. 1c).

The first endodontic files were manufactured in stainless steel and used manually. Since the end of 1980s, nickel-titanium engine-driven rotary instruments are commercially distributed and used increasingly in the endodontic practice. Indeed, Ni-Ti alloys (a family of shape memory alloys—SMA) confer the files a great flexural ability thanks to their pseudoelastic behavior, i.e., a nonlinear elastic behavior that allows the material to undergo mechanically induced high deformations without plastic residual strain after stress removal. This characteristic behavior of SMA is due to a stress-induced reversible solid-solid phase transformation between two different crystallographic structures, austenite and martensite, which takes place when the working temperature is greater than a specific value for each alloy (called *austenite finish temperature*, A_f). The use of Ni-Ti on behalf of stainless steel is a great improvement for the treatment, as shown in this work. The unique drawback is the proneness of the Ni-Ti device to break without early warning sign. Accordingly, it could be very useful for the clinician to know if and when a repeated use of the files is allowed. Quite a lot of works devoted to give some indications to dentists are present in the literature on Ni-Ti instruments. In particular, many experimental studies were dedicated to evaluate their performance in terms of flexibility and torsional resistance (Ref 1-3). On the other hand, from the computational point of view, only three studies (Ref 4-6) based on finite element analyses (FEA) were conducted, aiming to evaluate some aspects of the mechanical behavior of the instruments (e.g., the stress distribution) related to their critical condition during root canal instrumentation and not assessable through laboratory or in vivo tests. In particular, Berutti et al. (Ref 4) and Xu and Zheng (Ref 5) proposed simple models of different Ni-Ti instruments not accurate in terms of files geometries, loading conditions, and materials constitutive models. To simulate realistic clinical conditions, recently Necchi et al. (Ref 6) created a more truthful model of a

This article is an invited paper selected from presentations at Shape Memory and Superelastic Technologies 2008, held September 21-25, 2008, in Stresa, Italy, and has been expanded from the original presentation.

Lorenza Petrini, Structural Engineering Department, Politecnico di Milano, Milan, Italy; **Silvia Necchi** and **Francesco Migliavacca**, Laboratory of Biological Structure Mechanics, Structural Engineering Department, Politecnico di Milano, Milan, Italy; and **Silvio Taschieri**, IRCCS Istituto Ortopedico Galeazzi, Health Technologies Department, Università degli Studi di Milano, Milan, Italy. Contact e-mail: lorenza.petrini@polimi.it.

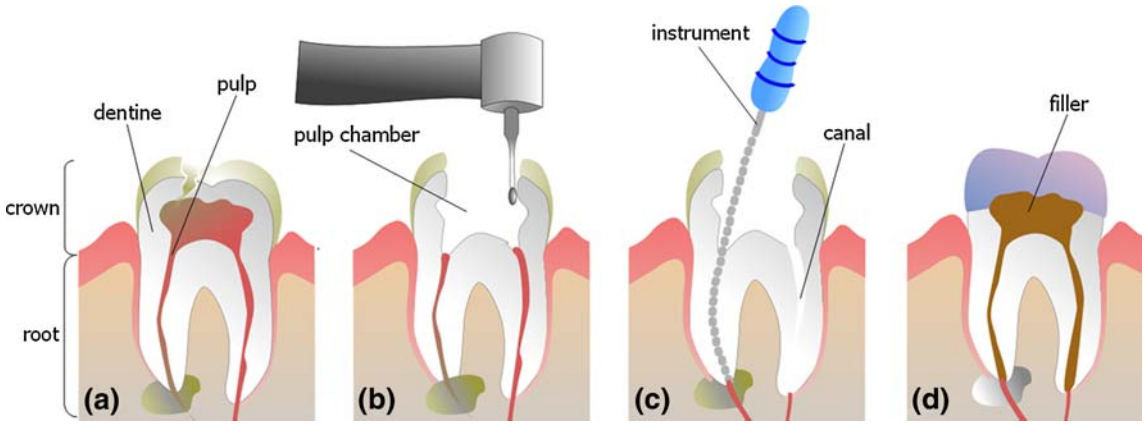

Fig. 1 Sketch of a tooth section with description of the endodontic treatment: unhealthy tooth (a), drilling (b), shaping (c), and obturation (d)

specific Ni-Ti instrument operating in a root canal. To reach this goal, the authors accurately reproduced the geometry of the instrument and different root canals. Furthermore, they used an advanced constitutive model for the Ni-Ti alloy. The stress that the instrument undergoes during clinical procedures (composed of continuous insertion and removal of the instrument in and out of the canal) was studied to evaluate the effects of the canal shape generated in the instrument.

In this work, the same authors intended to deepen the research previously presented on the subject by comparing the mechanical performance of three different Ni-Ti alloys when used to produce rotary endodontic instruments. Attention was paid to understand if an appropriate material choice may reduce the criticality of the treatment in particular clinical conditions. In fact, Ni-Ti alloys are characterized by strong dependence of the mechanical behavior on composition and working process. As a consequence, they give the possibility of "designing" the material according to the required device properties. Nevertheless, material and products are prone to anomalous mechanical behavior deriving from uncontrolled device production phases. The improvement in the technique due to SMA versus stainless steel employment was also underlined.

2. Numerical Modeling

The software Rhinoceros 2.0 Evaluation (Robert McNeel & Associates, Seattle, WA) was used for creating the geometrical model, while the commercial code ABAQUS 6.5-1/Standard (SIMULIA, Providence, RI) was employed for the computational analyses. In the following, the FE (finite element) model characteristics, in terms of geometry, material, boundary, and interaction conditions are described.

2.1 Geometrical Models and Meshes

The same 3D model of a ProTaper finisher file F1 (manufactured by Dentsply Maillefer Instruments—Ballaigues—Switzerland and used in final step of the shaping sequence) proposed in Necchi et al. (Ref 6) was used in this work. Figure 2 shows the main geometrical features of the instrument reproduced in the model. The handle part of the file does not serve any specific function in the shaping procedure, and therefore it was neglected in the numerical analyses. The created 3D geometrical model of the file was meshed using 10-nodes tetrahedral elements. A grid sensitivity study was performed to choose the most convenient number of elements (in terms of computational time and results accuracy) that was found in 5241, which assured an accurate description of sharp angles and curves.

The canals were modeled as simple rigid surfaces shaped as pipes (as described in the previous study), following a canal classification proposed in the literature (Ref 7), and based on radius, angle, and position of curvature. In this work, four types of canal geometries were considered (Fig. 3), characterized by a radius r of 2 or 5 mm, an angle α of 45° or 30°, and an apical or middle position (p) of the curvature. The 3D models of the canals were meshed using 4-node bilinear elements. A smooth discretization was used to prevent computational problems in the simulation during the contact between the canal wall and the file.

2.2 Materials Definition

Three Ni-Ti alloys, a *standard*, a *long*, and a *super* alloy, were considered, presenting a pseudoelastic behavior characterized by different values of hardening coefficient, limit transformation strain, and single-variant martensitic yielding stress and strain. In particular, the *standard alloy* resembles an alloy with mean properties and a transformation region amplitude of 7%. The *long alloy* resembles an ad hoc-designed material characterized by a wider transformation region (amplitude 9%) with respect to the *standard* one. The *super alloy* resembles a martensitic Ni-Ti alloy which underwent work-hardening during device production and hence shows an extended Hookian behavior without transformation region at any temperature (Ref 8). The stress-strain diagram describing the pseudoelastic behavior of the studied alloys is shown in Fig. 4. The mechanical parameters used for defining this behavior are listed in Table 1 and shown in Fig. 5. They are: the *transformation starting* and *finishing stress* (σ_{ts} and σ_{tf}, i.e., the stress values at which, at the working temperature, the transformation between austenite and single-variant martensite starts and finishes, respectively), the *limit transformation strain* (ε_L, i.e., the amplitude of the transformation strain interval), and the *martensitic yielding stress* and *strain* (σ_y^M and ε_y^M, the so-called *pseudoelastic limits*, i.e., the limit values over which the pseudoelastic behavior finishes). The respective values were arbitrarily imposed due to the impossibility of retrieving any information about the real materials used by the

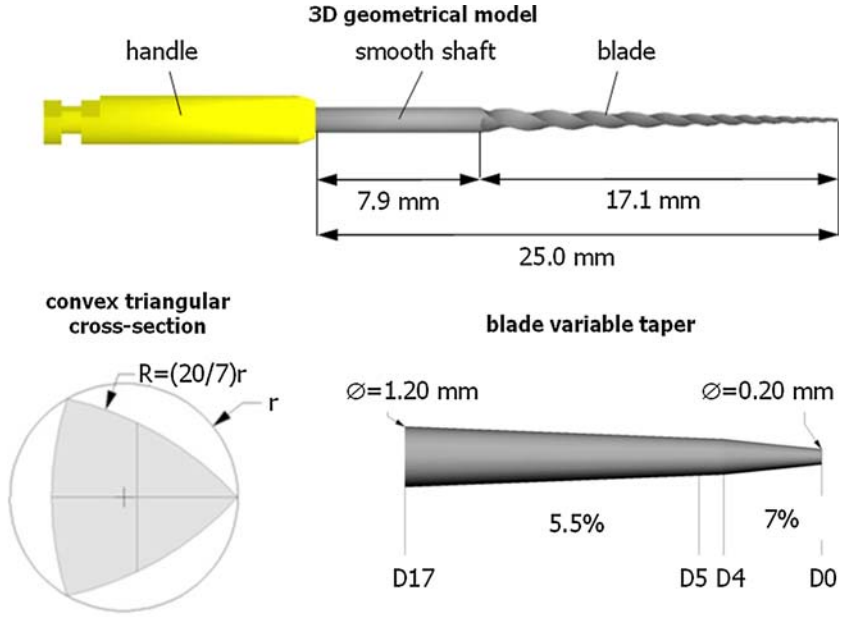

Fig. 2 Main geometrical features of the ProTaper F1 reproduced in the model

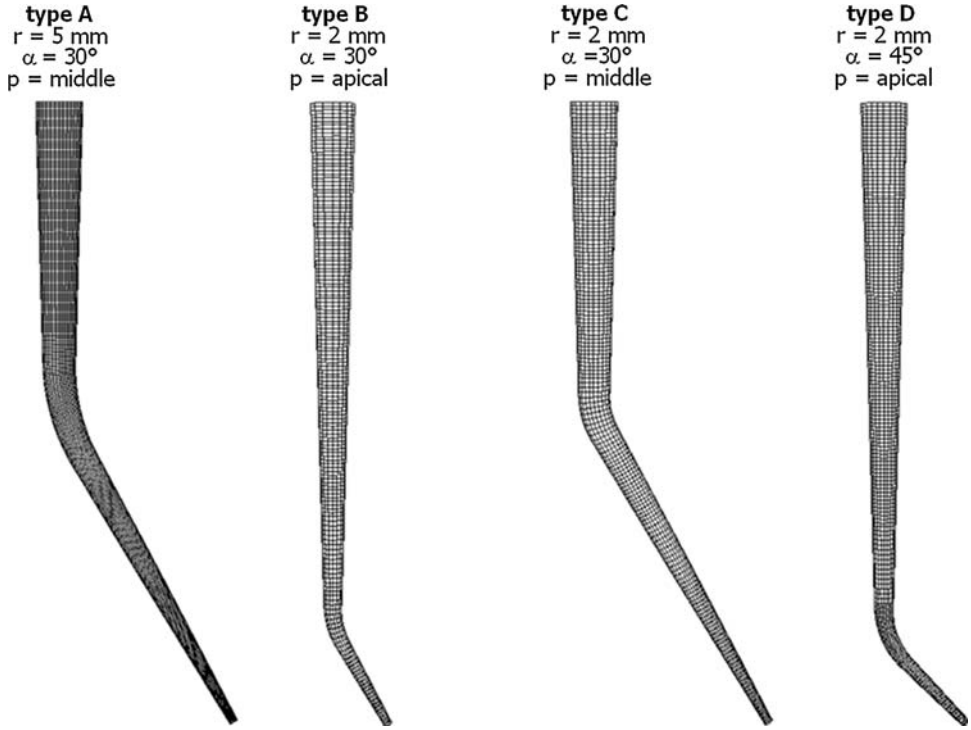

Fig. 3 Root canal geometries (meshed models)

instrument manufacturers. An ad hoc computational subroutine (Ref 9) was used to reproduce the complex thermomechanical behavior of the Ni-Ti alloys. Values of 25 and 10 °C were chosen for the working temperature and the temperature A_f, respectively. Since the used subroutine is not able to describe the plastic behavior following yielding of martensite, in this study, the simulation results were considered reliable only when stress and strain values were lower than the pseudoelastic limits. Moreover, the accumulation of plastic deformation due to cyclic loading in the pseudoelastic ranges was not accounted for.

AISI 316L stainless steel, widely used in biomedical applications, was employed as comparison material. The mechanical parameter values (Ref 10) are listed in Table 1 and the corresponding stress-strain diagram is reported in Fig. 4. For describing this behavior, an elastoplastic constitutive

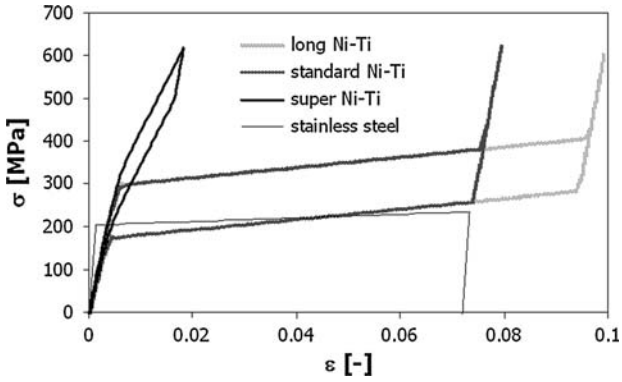

Fig. 4 Stress-strain diagram of the considered "ideal" Ni-Ti alloys and of a typical stainless steel

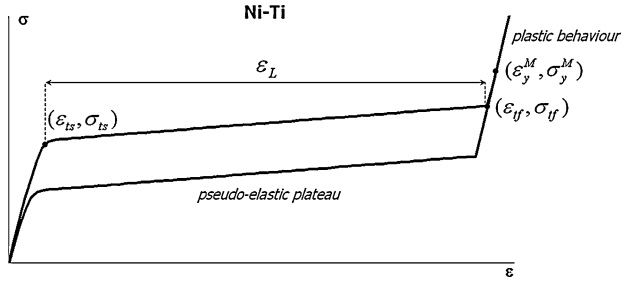

Fig. 5 Stress-strain diagram of the characteristic pseudoelastic behavior of SMA (ts = transformation starting, tf = transformation finishing, y = yield, L = limit)

Table 1 Values of stainless steel and Ni-Ti alloy characteristic mechanical parameters used in the numerical analyses

		Ni-Ti			
		Standard	**Long**	**Super**	**Stainless steel AISI 316L**
E, MPa	Young modulus	70,000	70,000	70,000	193,000
ν	Poisson ratio	0.3	0.3	0.3	0.3
σ_y^S, MPa	Yield stress	···	···	···	205
ε_y^S, %	Yield strain	···	···	···	0.1
σ_f, MPa	Fracture stress	···	···	···	515
ε_f, %	Fracture strain	···	···	···	60
H, MPa	Hardening parameter	1,000	1,000	30,000	520
σ_{ts}, MPa	Transformation starting stress	300	300	···	···
σ_{tf}, MPa	Transformation finishing stress	380	400	···	···
ε_L, %	Limit transformation strain	7	9	···	···
σ_y^M, MPa	Martensitic yielding stress	480	550	1,975	···
ε_y^M, %	Martensitic yielding strain	7.7	9.7	7.0	···

model with kinematic hardening, provided by the computational code library, was adopted.

2.3 Boundary and Interaction Conditions

The boundary and interaction conditions were imposed to simulate the clinical operating conditions (see Ref 6 for details). The modeled instruments were forced into the root canals until the apex was reached (*insertion* step) and immediately retrieved (*removal* step), while maintaining a continuous rotation around their longitudinal axis.

To avoid excessively long computational time, a rotational speed having an order of magnitude lower than the real one was imposed to the instruments. Moreover, as a first approach to the problem, neither friction nor machining action was considered between the instrument blade and the canal wall. A "soft" contact with an exponential pressure-overclosure model was imposed to simulate their interaction. Hence, the torsional stresses induced in the file during the procedure were neglected.

3. Results

The instruments performance was studied by analyzing the strain values reached during the phases of file insertion and removal into and out of the canals. The strain is a more accurate quantity to check. Indeed, the nonlinear behavior of both materials is mainly characterized by high increments of strain but small variations of stress for the presence of a wide region with low hardening modulus (corresponding to the transformation form austenite to single-variant martensite for Ni-Ti and to material plasticization for steel) in their stress-strain curves. In the following, this region will be indicated as "plateau."

For results evaluation, *equivalent strains*, given by the combination of the strain tensor components in all the directions ($\varepsilon^{eq} = \sqrt{(2/3)\boldsymbol{\varepsilon} : \boldsymbol{\varepsilon}}$), along with the *logarithmic maximum principal strain* ($\ln \lambda_{max}$) were calculated allowing to obtain scalar values to be compared with the limits derived from uniaxial tests.

In particular, the reference variables considered for the Ni-Ti alloys were ε_{tr}^{eq} (i.e., the instantaneous equivalent strain hoarded in the transformation plateau) and $\ln \lambda_{max}$ (i.e., the instantaneous maximum principal total strain the instruments undergoes, sum of the elastic, and the transformation component). The undeformed shape recovery after the removal step was considered assured if $\varepsilon_{tr}^{eq} \leq \varepsilon_L$. In the limit case of $\varepsilon_{tr}^{eq} = \varepsilon_L$, that means in the case of completed transformation, the additional condition $\ln \lambda_{max} \leq \ln(1 + \varepsilon_y^M)$ was required to be satisfied.

In the stainless steel case, ε_{pl}^{eq} (i.e., the instantaneous equivalent permanent deformation that appears whenever the yielding strain ε_y is reached) and $\ln \lambda_{max}$ (i.e., the instantaneous maximum principal total strain the instruments undergoes, sum of the elastic, and the plastic component) were considered.

The strain levels were analyzed mainly at the end of the insertion step, because it turned out as the more demanding condition for the materials. Table 2 provides the values obtained for the *logarithmic maximum principal strain* ($\ln \lambda_{max}$) and transformation (ε_{tr}^{eq}) or plastic (ε_{pl}^{eq}) strain in this configuration as a function of the considered material and canal type.

In the case of the Ni-Ti alloys, the $\ln \lambda_{max}$ value ranges are 6.6 to 8.4%, 6.6 to 9.0%, and 5.2 to 7.9% for the *standard*, the *long*, and the *super* alloy, respectively. Correspondingly, ε_{tr}^{eq} values range between 5.8 and 7.0% and between 5.8 and 8.6% for the *standard* and the *long* alloy (no equivalent transformation strain is produced in the case of *super* alloy).

Critical values of $\ln \lambda_{max}$ and ε_{tr}^{eq} were observed for both the *standard* and *super* alloys during insertion in canal type C (very sharp curvature in the medial part) which turned out to be the worst working condition. In this case, the recovery of the undeformed shape was not possible. Contrarily, the instrument with *long* alloy resulted as working in the material pseudo-elastic domain. Moreover, in every considered case, the *long* alloy furnished the better performance in terms of difference between the reached strain levels and the material critical thresholds ($\ln(1 + \varepsilon_y^M)$ and ε_L for $\ln \lambda_{max}$ and ε_{tr}^{eq}, respectively). Figure 6 shows the distribution of the total strain at the end of the insertion step in canal type C. Analyzing the answer of the different files to the variation of the curvature parameters, the *super* alloy results to be the most sensitive material in terms of reached $\ln \lambda_{max}$ values. Indeed, the percentage increases for the *standard*, *long*, and *super* alloys, respectively, were: (a) 27, 36, and 52% when shifting the radius from 5 to 2 mm (canal type A to type C); (b) 3, 18, and 21% changing the angle from 30° to 45° (canal type B to type D); and (c) 17, 23, and 36% when moving the curvature position from apical to medial (canal type B to type C). In terms of ε_{tr}^{eq}, the comparison between the *standard* and the *long* alloy indicates the second as the more sensitive to the variation of the canal parameters. In fact, the following respective increments were recorded for these alloys: (a) 21% and +48% when shifting the radius from 5 to 2 mm (canal type A to type C); (b) 3% and +5% changing the angle from 30° to 45° (canal type B to type D); and (c) 9 and 16% when moving the curvature position from apical to medial (canal type B to type C).

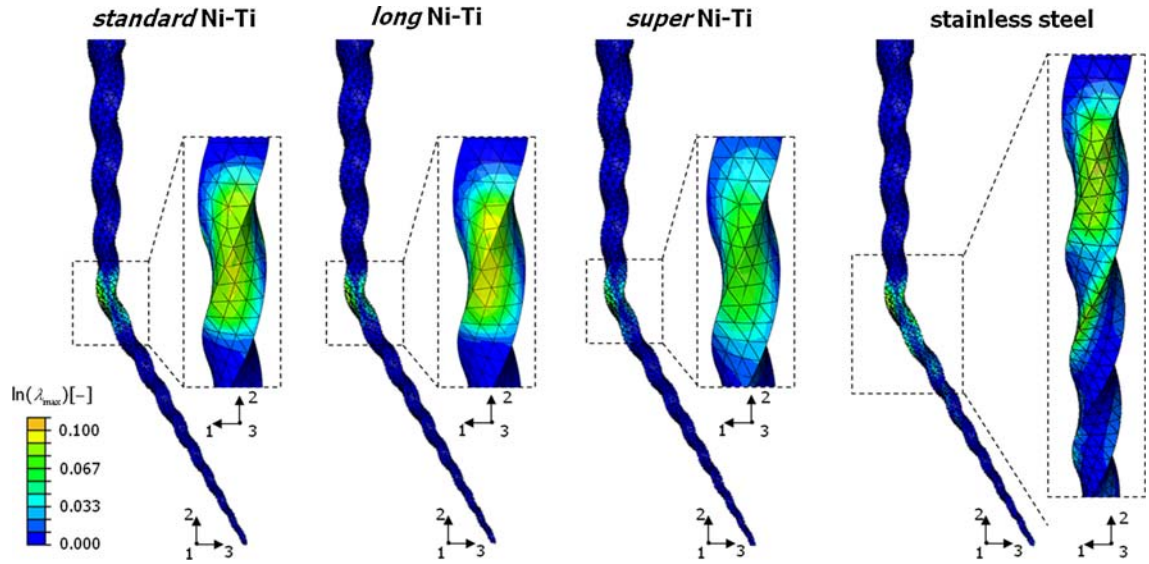

Fig. 6 End of insertion step, canal type C: logarithmic maximum principal strain levels reached in Ni-Ti and stainless steel instruments

Table 2 Percentage values obtained for the specific variables concerning Ni-Ti (logarithmic maximum principal strain $\ln \lambda_{max}$ and equivalent transformation strain ε_{tr}^{eq}) and stainless steel (logarithmic maximum principal strain $\ln \lambda_{max}$ and equivalent plastic strain ε_{pl}^{eq}) at the end of the insertion step

				Ni-Ti						
	Parameters			Standard		Long		Super	Stainless steel	
Canals	*r*	α, °	*p*	$\ln \lambda_{max}$	ε_{tr}^{eq}	$\ln \lambda_{max}$	ε_{tr}^{eq}	$\ln \lambda_{max}$	$\ln \lambda_{max}$	ε_{pl}^{eq}
A	5	30	m	6.6	5.8	6.6	5.8	5.2	7.1	7.1
B	2	30	a	7.2	6.4	7.3	7.4	5.8	10.2	10.0
C	2	30	m	8.4	7.0	9.0	8.6	7.9	10.9	11.5
D	2	45	a	7.4	6.6	8.6	7.8	7.0	12.1	11.9

The canal parameters refers to the radius (2 or 5 mm), the angle (30° or 45°), and the position (apical or medial) of the curvature

Table 3 Percentage of variation in the strain variables as function of the curvature parameters for the Ni-Ti and the stainless steel instruments

		Ni-Ti						
		Standard		Long		Super	Stainless steel	
Canals	Parameters	ln λ_{max}, %	ε_{tr}^{eq}, %	ln λ_{max}, %	ε_{tr}^{eq}, %	ln λ_{max}, %	ln λ_{max}, %	ε_{pl}^{eq}, %
A vs. C	*r*: 2 vs. 5 mm	+27	+21	+36	+48	+52	+54	+62
D vs. B	α: 45° vs. 30°	+3	+3	+18	+5	+21	+19	+19
C vs. B	*p*: m vs. a	+17	+9	+23	+16	+36	+7	+15

In the case of stainless steel, the instrument underwent critical total strain levels, reaching values of the *logarithmic principal strain* (ln λ_{max}) well beyond the yielding strain (ε_y^S), varying between 7.1 and 12.1%. ε_{pl}^{eq} ranged between 7.1 and 11.9%. From the studied cases, the most critical condition resulted in the canal type D. As a function of the curvature parameters, ln λ_{max} and ε_{pl}^{eq} increased of: 54 and 62% shifting the radius from 5 to 2 mm, 19% changing the angle from 30° to 45°, 7 and 15% moving the curvature position from apical to medial.

The depicted results (Table 3) clearly indicate that, for all the considered material, in the canal comparison, the primary curvature parameter influencing the mechanical behavior of the instrument (higher variations of strain) is the radius of curvature. Differently, the second dominant parameter is judged the position of curvature for the Ni-Ti alloys and the angle of curvature for the stainless steel.

The values of ln λ_{max} obtained for the stainless steel file were higher in every canal compared to the Ni-Ti instrument (see Fig. 6). Moreover, the stainless steel instruments showed a lower ability to conform to the canal shape during an entire insertion-removal cycle. In particular, the tip of the stainless steel file plasticized just after the first contact with the canal wall, determining successive irregular interactions between the file and the wall, and inducing the instrument to work in the plastic range of the material for the larger portion of the treatment duration. The Ni-Ti file, instead, bends uniformly along the blade, following the original curvature of the canal. This behavior was shown independently by the canal geometry.

4. Discussion and Conclusions

FEA are recognized to have an important role in optimizing the behavior of biomedical devices. In this work, focused on the study of the mechanical performance of a Ni-Ti rotary endodontic instrument, attention was mainly paid to understand the effects of the materials choice in the endodontic treatment and those of a not correct production on the performance of the file. Three types of alloys were considered. The clinical operating conditions were simulated by imposing a combined movement of translation and rotation of the instrument into and out of canal root. Four geometries of canals, differing in their curvature features, were taken into account. Flexural strains varying cyclically during rotation of the endodontic instrument were analyzed.

The results from the simulations suggest that Ni-Ti alloys are good materials for the production of engine-driven rotary instruments, especially if compared to stainless steel. As expected, the Ni-Ti files showed high flexibility during the transformation of the alloy from austenite to single-variant martensite. Considering the *standard* alloy, only in the case of a very sharp curvature in the medial part of the canal, the plastic domain was reached. In the case of *super* alloy, the martensitic yielding strain was reached when the instrument operated in canals with a small radius curvature having a sharp angle in the medial position or a more obtuse angle in the apical position. On the contrary, the *long* alloy always worked in its pseudoelastic domain. The stainless steel instrument plasticized after the first contact with the canal wall and continued building up plasticity. These results suggest that the use of a Ni-Ti alloy with a wide pseudoelastic plateau should be advisable to prevent damages to the instruments causing clinical failures. Moreover, they confirmed the literature outcomes (Ref 5, 6, 11-15) indicating that sharp medial curvatures of the canals represent the most demanding conditions for the instruments.

Three main limitations can be recognized in the proposed model. First, in the implemented Ni-Ti constitutive model, the material was assumed to be indefinitely elastic (once completed the transformation from austenite and single-variant martensite) and the accumulation of plastic deformation due to cyclic loading in the pseudoelastic ranges was not accounted for. This limitation can cause underestimation of deformation levels. Moreover, hypothetical values were imposed to the mechanical parameters of the alloys: the knowledge of the exact physical and mechanical characteristics of the Ni-Ti alloys used by manufacturers could improve the results.

Second, a reduced rotational speed was imposed to the instrument: in real conditions, it implies a smaller number of cycles and a lower strain rate, affecting the fatigue behavior of the instruments. Nevertheless, in our simulations, this restriction affected the results of stainless steel, providing low values for the accumulated plastic deformations, while it was not significant for SMA, because of the omission of the plastic deformation accumulation phenomenon and strain rate influence in the material model.

Last, the study of torsional stresses induced in the instruments during instrumentation or generated during critical clinical events such as locking of the file tip into the dentine was not taken into account. Overcoming this limitation could allow to describe more precisely the file behavior and to give indications about the failure mode which seems to be given by the interaction (Ref 3, 16-18) between flexural and torsional fatigue (Ref 7, 19-24) and overloading (Ref 25, 26).

However, even under the highlighted limitations, the developed model demonstrated to be a useful tool to compare the behavior of Ni-Ti instrument differing in their material characteristics and can be considered promising in helping the instrument design.

Acknowledgments

The authors would like to thank Daniele Aspesi, MEng, for his contribution to the numerical analyses. Part of this work has been carried out under the financial auspices of the Italian Ministry for Research and Higher Education (MiUR—Ministero dell'Universita e della Ricerca) through the PRIN 2006 Project: "Shape memory alloy active microactuators and devices for biomedical applications: constitutive modeling, structural analysis, design, use of laser techniques for prototype implementation and experimental validation". Such support is gratefully acknowledged by the authors.

References

1. M. Hülsmann, O.A. Peters, and P.M.H. Dummer, Mechanical Preparation of Root Canals: Shaping Goals, Techniques and Means, *Endod. Top.*, 2005, **10**, p 30–76
2. S. Taschieri, S. Necchi, G. Rosano, M. Del Fabbro, R. Weinstein, and P. Machtou, Avantages et limites des instruments en nickel-titane pour la préparation canalaire endodontique. Revue de la littérature récente (Advantages and limits of nickel-titanium instruments for root canal preparation. A review of the current literature), *Schweiz. Monatsschr. Zahnmed.*, 2005, **115**, p 1000–1005 (in French)
3. M.G. Bahia, M.C. Melo, and V.T. Buono, Influence of Cyclic Torsional Loading on the Fatigue Resistance of K3 Instruments, *J. Endod.*, 2008, **41**, p 883–891
4. E. Berutti, G. Chiandussi, I. Gaviglio, and A. Ibba, Comparative Analysis of Torsional and Bending Stresses in Two Mathematical Models of Nickel-Titanium Rotary Instruments: ProTaper Versus ProFile, *J. Endod.*, 2003, **29**, p 15–19
5. X. Xu and Y. Zheng, Comparative Study of Torsional and Bending Properties for Six Models of Nickel-Titanium Root Canal Instruments with Different Cross-Sections, *J. Endod.*, 2006, **32**, p 372–375
6. S. Necchi, S. Taschieri, L. Petrini, and F. Migliavacca, Mechanical Behaviour of Ni-Ti Rotary Endodontic Files in Simulated Clinical Conditions: A Computational Study, *Int. Endod. J.*, 2008, **41**, p 939–949
7. J.P. Pruett, D.J. Clement, and D.L. Carnes, Cyclic Fatigue Testing of Nickel Titanium Endodontic Instruments, *J. Endod.*, 1997, **23**, p 77–85
8. G.R. Zadno and T.W. Duerig, Linear and Non-Linear Superelasticity in NiTi, *MRS Shape Memory Mater.*, 1989, **9**, p 201–206. Also available on www.nitinol.com
9. F. Auricchio and L. Petrini, A Three-Dimensional Model Describing Stress-Temperature Induced Solid Phase Transformations: Solution Algorithm and Boundary Value Problems, *Int. J. Numer. Methods Eng.*, 2004, **61**, p 716–737
10. F. Auricchio, M. Di Loreto, and E. Sacco, Finite-Element Analysis of a Stenotic Artery Revascularization Through a Stent Insertion, *Comput. Methods Biomech. Biomed. Eng.*, 2001, **4**, p 249–263
11. Y. Haikel, R. Serfaty, G. Bateman, B. Senger, and C. Allemann, Dynamic and Cyclic Fatigue of Engine-Driven Rotary Nickel-Titanium Endodontic Instruments, *J. Endod.*, 1999, **25**, p 434–440
12. G. Zelada, P. Varela, B. Martín, J.G. Bahíllo, F. Magán, and S. Ahn, The Effect of Rotational Speed and the Curvature of Root Canals on the Breakage of Rotary Endodontic Instruments, *J. Endod.*, 2002, **28**, p 540–542
13. U.M. Li, B.S. Lee, C.T. Shih, W.H. Lan, and C.P. Lin, Cyclic Fatigue of Endodontic Nickel Titanium Rotary Instruments: Static and Dynamic Tests, *J. Endod.*, 2002, **28**, p 448–451
14. B. Martín, G. Zelada, P. Varela, J.G. Bahíllo, F. Magán, S. Ahn, and C. Rodríguez, Factors Influencing the Fracture of Nickel-Titanium Rotary Instruments, *J. Endod.*, 2003, **36**, p 262–266
15. H.P. Lopes, E.J. Moreira, C.N. Elias, R.A. de Almeida, and M.S. Neves, Cyclic Fatigue of ProTaper Instruments, *J. Endod.*, 2007, **33**, p 55–57
16. C.J. Ullmann and O.A. Peters, Effect of Cyclic Fatigue on Static Fracture Loads in ProTaper Nickel-Titanium Rotary Instruments, *J. Endod.*, 2005, **31**, p 183–186
17. M.G. Bahia, M.C. Melo, and V.T. Buono, Influence of Simulated Clinical Use on the Torsional Behavior of Nickel-Titanium Rotary Endodontic Instruments, *Oral Surg. Oral Med. Oral Pathol. Oral Radiol. Endod.*, 2006, **101**, p 675–680
18. F.O.G. Barbosa, J.A.C. Ponciano, and M.C.P. Araújo, Influence of Previous Angular Deformation on Flexural Fatigue Resistance of K3 Nickel–Titanium Rotary Instruments, *J. Endod.*, 2007, **33**, p 1477–1480
19. B. Sattapan, J.E. Palamara, and H.H. Messer, Torque During Canal Instrumentation Using Rotary Nickel-Titanium Files, *J. Endod.*, 2000, **26**, p 156–160
20. D. Fife, G. Gambarini, and L.R. Britto, Cyclic Fatigue Testing of ProTaper NiTi Rotary Instruments After Clinical Use, *Oral Surg. Oral Med. Oral Pathol. Oral Radiol. Endod.*, 2004, **97**, p 251–256
21. G. Yared, In Vitro Study of the Torsional Properties of New and Used ProFile Nickel Titanium Rotary Files, *J. Endod.*, 2004, **30**, p 410–412
22. M.G. Bahia and V.T. Buono, Decrease in the Fatigue Resistance of Nickel-Titanium Rotary Instruments After Clinical Use in Curved Root Canals, *Oral Surg. Oral Med. Oral Pathol. Oral Radiol. Endod.*, 2005, **100**, p 249–255
23. N.M. Grande, G. Plotino, R. Pecci, R. Bedini, V.A. Malagnino, and F. Somma, Cyclic Fatigue Resistance and Three-Dimensional Analysis of Instruments from Two Nickel–Titanium Rotary Systems, *Int. Endod. J.*, 2006, **39**, p 755–763
24. G.S.P. Cheung and B.W. Darvell, Fatigue Testing of a NiTi Rotary Instrument. Part 1: Strain-Life Relationship, *Int. Endod. J.*, 2007, **40**, p 626–632
25. S.B. Alapati, W.A. Brantley, T.A. Svec, J.M. Powers, J.M. Nusstein, and G.S. Daehn, SEM Observations of Nickel-Titanium Rotary Endodontic Instruments that Fractured During Clinical Use, *J. Endod.*, 2005, **31**, p 40–43
26. A.P. Spanaki-Voreadi, N.P. Kerezoudis, and S. Zinelis, Failure Mechanism of ProTaper Ni-Ti Rotary Instruments During Clinical Use: Fractographic Analysis, *Int. Endod. J.*, 2006, **39**, p 171–178